Detection of Pores in Additive Manufactured Parts by Near Field Response of Laser-Induced Ultrasound

Timothy A Bigelow[1,2, a)], Benjamin Schneider[1, b)], and Hossein Taheri[2,3, c)]

[1]*Department of Electrical and Computer Engineering, Iowa State University, 1915 Scholl Road, Ames, IA, 50011.*
[2]*Department of Mechanical Engineering, Iowa State University, 1915 Scholl Road, Ames, IA, 50011.*
[3]*Department of Manufacturing Engineering, Georgia Southern University, P.O. Box 7991, Statesboro, GA 30460.*

[a)]Corresponding author: bigelow@iastate.edu
[b)]bjs1@iastate.edu
[c)]htaheri@georgiasouthern.edu

Abstract. In-line monitoring of 3D printed parts is vital if quality is to be maintained with this new manufacturing modality. Specifically, the reliable detection of pores in printed parts is vital if the finished products are to have the desired strength characteristics. In this work, we utilize COMSOL(Burlington, MA) to numerically compare a new detection method where the interferometer and laser-generated ultrasound are focused at the same spatial location. The changes in the surface response to defects in the near-field of the induced ultrasound wave are then assessed as a function of defect size and depth. Our numerical results demonstrated that the impact of defects was easier to visualize when quantifying the surface velocity as opposed to surface displacement. The amplitude of the difference is comparable to that observed when utilizing scattering of the Rayleigh wave in the detection. However, the new approach does not require a 1 mm separation between the laser-generating ultrasound spot and the interferometer improving the spatial resolution of the detection.

INTRODUCTION

Additive manufacturing will have a significant impact on production in the future. However, numerous defects such as porosity due to trapped gas or lack-of-fusion can significantly impact the strength of the finished part [1]. Currently, the variability in porosity even for identical build parameters is one of the greatest technical challenge limiting the additive manufacturing revolution. The current method for controlling porosity in a laser sintered part is to either use hot isostatic pressing after fabrication until the desired porosity is achieved or to tightly control the processing parameters/powder quality in an effort to ensure low porosity [2-5]. However, this is an open loop process with no guarantee that every part or portion of a part has a sufficiently low porosity for the intended mechanical load. While it may be possible to conduct non-destructive evaluation of the printed part post fabrication, this is not a trivial endeavor. X-ray CT could reveal the location and number density of the pore in the part, but could not be used with most large metal parts due to the density of the metals and the spatial resolution needed to find the pores. Ultrasound evaluation of porosity post-fabrication is also challenging due to the anticipated complex geometries making propagation of the ultrasound waves in the part challenging to model and interpret. Therefore, being able to detect pores in manufactured parts during the build will enable improved efficiency while maintain safety.

Considerable work has been conducted on using laser-based ultrasound to detect isolated pores in laser sintered parts [6-10]. Specifically, a laser is used to generate a Rayleigh wave along the surface of the part. A second laser interferometer is then used to detect the scattering of the wave from sub-surface defects. Pores with diameters on the order of 100 μm can be detected up to a depth of about 200 μm using this approach with larger pores, ~700 μm diameter, detectable at depths up to 800 μm [6]. While the prior work establishes a method for the detection of some defects, it does not meet the requirements for optimal quality control of laser sintered parts as the transmitting and detection laser need to be separated by at least 1 to 3 mm.

In our work, we assessed the possibility of detecting pores when the ultrasound generating laser and the interferometer were focused at the same spot. Defect detection was then based on a change in the surface response due to the presence of a pore just below the surface. The impact of the defect size and depth on the response were then quantified via finite element modelling. Hutchins et al previously demonstrated that changes in the surface geometry can impact ultrasound generation by the laser [11]. However, their work focused on the impact of adding a coating to constrain the outer surface rather than our work where the pore would add an additional free surface near the boundary.

FINITE ELEMENT MODELS

COMSOL (Burlington, MA) was used to numerically model the generation and propagation of the elastic waves in the material. The waves were generated by modelling the thermal expansion resulting from an Nd:YAG lamp-pumped solid state laser focused on a stainless steel (SST 17-4PH) surface. The material properties used in the model are given in Table 1. The multiphysics capabilities of COMSOL were utilized, and the model included solid mechanics, heat transfer, and thermal expansion with temperature coupling. Finite Element Modelling (FEM) has been used frequently in the past to model the generation of elastic waves in this manner [12-14].

TABLE 1. Material properties used for stainless steel (SST 17-4PH) in our model. The shear and longitudinal wave speeds used in the model were experimentally determined from 3D printed samples in our lab.

Material Property	Parameter Value
Heat Capacity at Constant Pressure	475 J/(kg-K)
Thermal Conductivity	44.5 W/(m-K)
Coefficient of Thermal Expansion	12.3×10^{-6}/K
Density	7750 kg/m^3
Shear Wave Speed	3120 m/s
Longitudinal Wave Speed	5880 m/s
Young's Modulus	196.76 GPa
Poisson's Ratio	0.30406

Our FEM model was a two-dimensional axial symmetric model with a mesh size ranging from 3 to 17 μm. An example mesh for a pore size of 100 μm is shown in Fig 1.

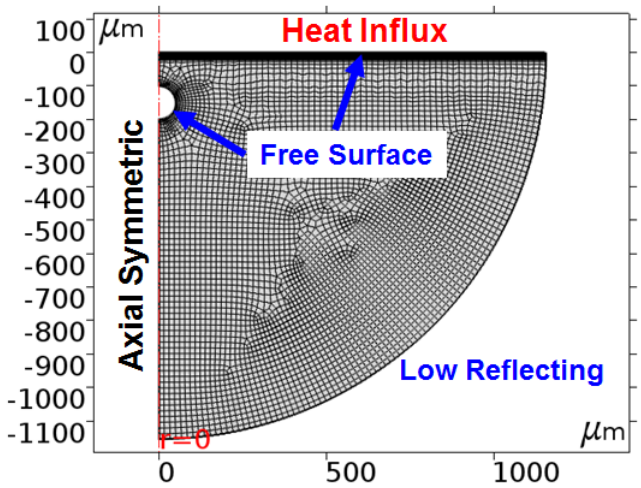

FIGURE 1. Example FEM mesh used to model the generation and propagation of the elastic waves in our study. This mesh was generated for a 100 μm pore located 100 μm below the surface.

In order to accurately capture the sharp changes in temperature and associated thermal expansion near the surface, the model also included a boundary layer with an initial thickness of 0.05 μm a stretch factor of 1.15 and an overall

thickness of 30 elements. If the mesh size is too large near the surface, the model can result in physically impossible results such as negative absolute temperatures. The mesh was refined until consistent and physically reasonable results were obtained.

The acoustic boundary conditions for the mesh consisted of a low reflecting boundary along the bottom of the simulated region to allow the waves to propagate out of the region of interest without back reflection. The remaining two surfaces for the surface of the metal and the pore were modelled as free surfaces. For the thermal modelling, the incident laser beam was modelled as a heat influx while the lower curved boundary assumed negligible heat flow. The pore boundary and top surface also acted as radiating boundaries with an emissivity of 0.8.

The models consisted of a single spherical pore located directly beneath the incident laser pulse. The diameter of the pore was varied from 25 μm to 500 μm while the depth of the pore was varied from 25 to 600 μm as measured from the top of the pore to the surface of the metal. The change in normal surface velocity relative to the surface velocity when no defect was present was then compared for the different pore depths and sizes. Surface velocity was selected instead of surface displacement as the large displacement due to the initial thermal expansion, and is subsequent slow return to normal, masked the displacements due to the presence of the pore. In practice, the surface normal velocity can be obtained by taking the time derivative of the displacement using a basic laser interferometer or one could use a Sagnac interferometer whose output is directly proportional to surface velocity [2].

The laser pulse had a duration of 11 ns and a Gaussian beam shape was assumed as given by

$$I(r) = I_o \exp\left(-\frac{r^2}{2r_{spot}^2}\right) \tag{1}$$

where r is the distance from the beam axis along the surface of the metal, I_o is the peak laser intensity of the surface, and r_{spot} is the spot size. For our simulations, I_o was set to 8.17 W/m^2 which was just below the ablation threshold so that we could remain in the elastic regime and r_{spot} was 100 μm. The maximum temperature on the surface of the metal due to the laser pulse is shown in Fig 2. The temperature decays quickly away from the top surface.

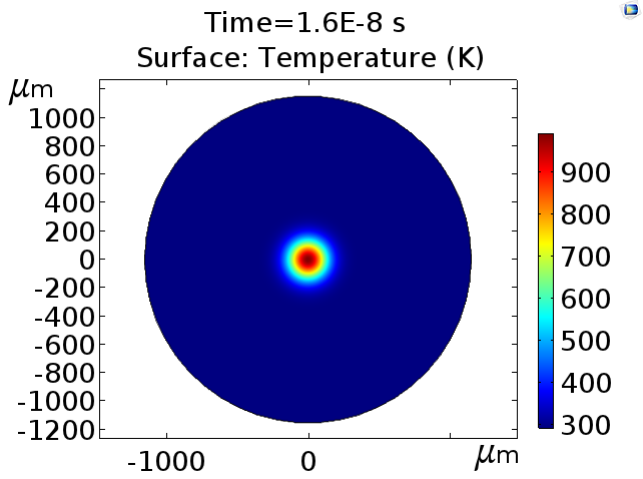

FIGURE 2. Peak temperature profile on the surface of the metal showing the range and distribution of the temperature increase across the surface.

RESULTS

Figure 3 shows the maximum difference in the normal velocity for different pore sizes and pore depths relative to when no pore is present. The results are presented in terms of both the absolute difference in cm/s as well as the percentage difference relative to the largest velocity of the surface following the laser when no defect is present. Larger shallower pores have a much stronger response than smaller and/or deeper pores. Also, while it is difficult to speculate on detection sensitivity from these numerical results, there is a clear difference in the surface response for pores on the order of 100 to 200 μm in diameter at depths of 100 μm. Therefore, the sensitivity appears to be

comparable to the traditional pore detection method based on Rayleigh waves. However, this needs to be confirmed experimentally.

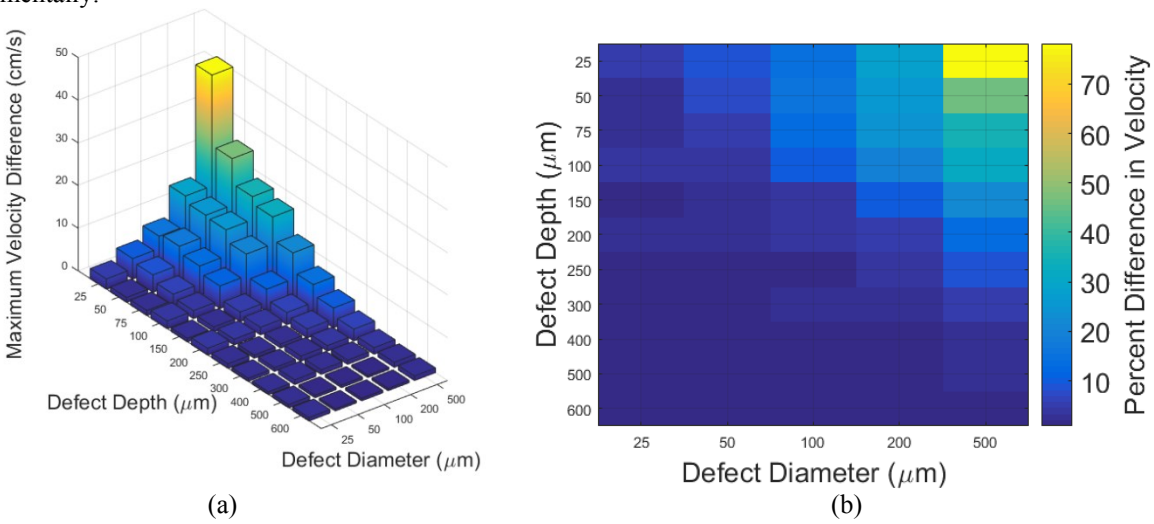

FIGURE 3. The maximum absolute difference (a) and percent difference (b) between the surface velocity when a pore is present relative to no pore for varying pore sizes and depths. The percent difference was found by dividing the absolute difference by the maximum velocity of the surface when no pore was present.

If we examine the waveform data more closely, as shown in Fig 4, the maximum difference in the velocity profile occurs shortly after the initial thermal expansion due to the laser pulse. Both the homogeneous case and the presence of the pore have a slight positive normal velocity component on the order of 10 cm/sec. However, the presence of the pore results in a larger velocity increases followed by a more rapid falloff of the velocity. This difference in amplitude and shape will result in a distinct signature signal when a pore is present.

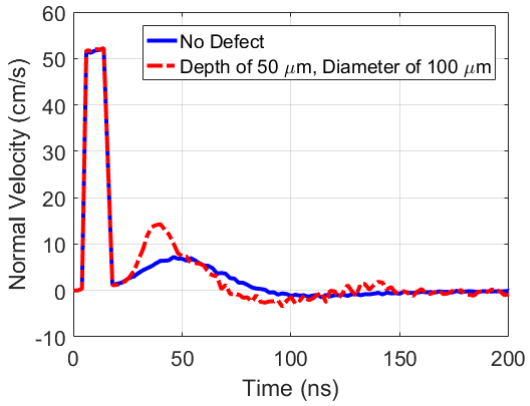

FIGURE 4. Example normal velocity profile directly above the pore for a pore size of 100 mm and a depth of 50 mm. The surface response with no defect present is also shown.

DISCUSSION/CONCLUSIONS

In this study, we demonstrated the feasibility of positioning the laser spot for the ultrasound generating laser and the interferometer at the same location. The sensitivity using the new approach is comparable to that observed when utilizing scattering of the Rayleigh wave in the detection. However, the new approach does not require a 1 to 3 mm separation between the laser-generating ultrasound spot and the interferometer improving the spatial resolution of the detection. As was observed when using laser-induced Rayleigh wave detection, shallower/larger defects have a greater impact on the velocity difference than smaller/deeper defects.

Even though the feasibility of the new approach was demonstrated, the present study has several short comings that need to be addressed before a fair comparison can be made to the traditional Rayleigh wave approach. First, the current study did not include any surface roughness. Change in the surface will likely have an impact on the surface response that might mask the response of the pore. This will reduce the sensitivity of the approach making smaller/deeper defects more difficult to detect. Second, the results were obtained solely from computer models. Experimental verification of the models are needed to confirm the numerical results. While it may not be feasible to test the smaller defects given the difficulty in controlling pore size and placement when the pores are on the order of the print resolution of the system, results for the larger pores can be compared to our numerical results to validate the technique. Lastly, the current results only compared the velocity difference at a single point of the numerical simulation. The receive characteristics of the interferometer should also be included when assessing the sensitivity of the technique to varying defect sizes and depths.

ACKNOWLEDGMENTS

This work was performed with support from National Science Foundation CMMI Award Number 1661146.

REFERENCES

1. H. Taheri, M. R. B. M. Shoaib, L. W. Koester, T. A. Bigelow, P. C. Collins and L. J. Bond, Int. J. Additive and Subtractive Materials Manufacturing **1** (2), 172-209 (2017).
2. S. Ziegelmeier, P. Christou, F. Wöllecke, C. Tuck, R. Goodridge, R. Hague, E. Krampe and E. Wintermantel, Journal of Materials Processing Technology **215**, 239-250 (2015).
3. T. Furumoto, A. Koizumi, M. R. Alkahari, R. Anayama, A. Hosokawa, R. Tanaka and T. Ueda, Journal of Materials Processing Technology **219**, 10-16 (2015).
4. J. A. Slotwinski, E. J. Garboczi and K. M. Hebenstreit, Journal of Research of the National Institute of Standards and Technology **119**, 494-528 (2014).
5. K. Shahzad, J. Deckers, J.-P. Kruth and J. Vleugels, Journal of Materials Processing Technology **213** (9), 1484-1494 (2013).
6. D. Cerniglia, M. Scafidi, A. Pantano and J. Rudlin, Ultrasonics **62**, 292-298 (2015).
7. M. Klein and J. Sears, *Proceedings of the 23rd International Congress on Applications of Lasers and Electro-Optics*, San Francisco, CA, 2004, Vol. 97, pp. 23.
8. S. P. Santospirito, R. Łopatka, D. Cerniglia, K. Słyk, B. Luo, D. Panggabean and J. Rudlin, *Proc. SPIE 8611, Frontiers in Ultrafast Optics: Biomedical, Scientific, and Industrial Applications XIII*, San Francisco, CA, 2013, SPIE, Vol. 8611, pp. 86111N.
9. J. Rudlin, D. Cerniglia, M. Scafidi and C. Schneider, *11th European Conference on Non-Destructive Testing (ECNDT 2014)*, Prague, Czech Republic, 2014.
10. S. Everton, P. Dickens, C. Tuck and B. Dutton, *Proceedings Volume 9353, Laser 3D Manufacturing II*, San Francisco, CA, 2015, SPIE, Vol. 9353, pp. 935316.
11. D. A. Hutchins, R. J. Dewhurst and S. B. Palmer, J. Acoust. Soc. Am. **70** (5), 1362-1369 (1981).
12. Z. Yunjie, G. Xiaorong, L. Lin, P. Yongdong and Q. Chunrong, Journal of Nondestructive Evaluation **36** (4), 70 (2017).
13. P. Liu, A. W. Nazirah and H. Sohn, Ultrasonics **69**, 248-258 (2016).
14. W. Liu and J.-W. Hong, Ultrasonics **55** (0), 113-122 (2015).